Research Article

Tim Enzlberger Jensen*

Spatial resolution of airborne gravity estimates in Kalman filtering

https://doi.org/10.1515/jogs-2022-0143
received September 3, 2021; accepted October 26, 2022

Abstract: Airborne gravimetry is an efficient and reliable method to obtain information on the gravity field, fundamental to gravity field modelling, geoid determination, and flood risk mapping. In evaluation and utilization of gravity estimates, two measures are of fundamental importance, namely the accuracy and spatial resolution. These measures are related to one another through the filtering required to suppress observational noise. As strapdown inertial measurement units (IMUs) are increasingly deployed for airborne gravity surveys, the Kalman filter estimation method is routinely used for gravity determination. Since filtering is not applied directly to the observations in Kalman filtering, it is not straightforward to associate the derived gravity estimates with a measure of spatial resolution. This investigation presents a method for deriving spatial resolution by evaluating the transfer function formed after applying a delta function to the observed accelerations. The method is applied to Kalman-filter-derived gravity estimates from an airborne strapdown IMU system, yielding a full-wavelength spatial resolution of 5.5 km at an accuracy of 0.6 mGal. These results are consistent with a comparison with upward continued terrestrial gravity observations.

Keywords: airborne gravimetry, Kalman filtering, spatial resolution, strapdown IMU

1 Introduction

Airborne gravity observations became an operational procedure in the 1990s with the advent of the Global Positioning System (Brozena 1992). Since then, the technique has proven itself reliable in mapping large areas of the Earth's gravity field efficiently and inexpensively (Gumert et al. 1991, Forsberg et al. 2001, Hwang et al. 2007, Fauzi Nordin et al. 2016, Scheinert et al. 2016, Huang et al. 2017). As with any other digital instrument, observations are not taken instantaneously and continuously, but at discrete sampling intervals. The spatial resolution of the derived gravity estimates is thus dependent on the aircraft's speed. Moreover, as the observations contain noise originating from both instrument and aircraft dynamics, the final resolution depends also on the amount of filtering required to suppress the observational noise. For this reason, the spatial resolution of airborne gravity estimates does not equal that of point-wise terrestrial observations, which can be spaced sufficiently close together at the cost of increased operational effort.

Marine gravimetry is similarly capable of efficiently mapping wide areas of the Earth's gravity field and generally results in superior accuracy and resolution due to the slower movement of the vehicle (Vaníček and Kingdon 2015, Lu et al. 2019). At sea, the gravimeter is much closer to the surface of the Earth, meaning that the possible resolution is not limited by the attenuation of the gravity field with altitude. Airborne observations are, however, not constrained to oceanic areas and are capable of mapping remote or inaccessible areas far from civilization. Moreover, airborne gravimetry is currently the only technique capable of mapping the coastal areas not accessible from either land or sea. Since knowledge of the gravity field is necessary to determine flooding risk and most of the Earth's population is situated along coastal areas, airborne gravimetry is an important component in modern infrastructure (Forsberg et al. 2000, Novák et al. 2003, National Research Council of the National Academies 2009, Muis et al. 2017).

Satellite observations are capable of mapping the entire surface of the Earth with a uniform resolution. However, the spatial resolution of these gravity estimates is limited by the attenuation of gravity at orbit altitude. Airborne gravimetry thus covers an important gap, not only in terms of spatial coverage but also in terms of spatial resolution. One might figuratively say that airborne gravimetry provides the glue for merging terrestrial

* **Corresponding author: Tim Enzlberger Jensen,** National Space Institute, Technical University of Denmark (DTU Space), Kgs. Lyngby, Denmark, e-mail: timj@space.dtu.dk

and space-borne gravity observations (Sproule et al. 2001, Kern et al. 2003, Forsberg et al. 2015).

The usefulness of airborne gravity estimates is thus determined not only by their accuracy but also by their spatial resolution. Since the signal-to-noise ratio can be thousands or more, the filtering of airborne observations is essential to obtain useful gravity estimates (Hammada 1996, Bruton 1997, Childers et al. 1999, Zhou and Cai 2013, Stepanov et al. 2015). Because the accuracy often improves with harder filtering, the gravity estimates are essentially a trade-off between accuracy and spatial resolution. Determining the spatial resolution of derived gravity estimates is thus equally important as determining the accuracy. This investigation presents a method of deriving the spatial resolution by considering the transfer function after applying a delta impulse to the observed accelerations. Such a method can be employed even when the convolution filter is unknown, e.g. as is the case in Kalman-filter-derived gravity estimates.

2 Airborne gravity estimates and spatial resolution

A modern airborne gravity system essentially consists of a gravimeter and a Global Navigation Satellite System (GNSS) receiver/antenna pair. Since the gravimeter is basically an accelerometer, the gravimeter on board an aircraft will sense specific force, $\mathbf{f}$, representing both gravity and kinematic accelerations originating from movement. Gravity estimates are derived from these observations as follows:

$$\mathbf{g} = \ddot{\mathbf{r}} - \mathbf{C}\mathbf{f}, \tag{1}$$

where $\ddot{\mathbf{r}}$ is the kinematic acceleration derived from GNSS position estimates and $\mathbf{C}$ is a rotation operator that projects the observed specific force onto the axes of a reference system with known orientation (Schwarz and Li 1997). In practice, the transformation can be accomplished either mechanically or computationally. The mechanical approach has been to place the gravimeter on a stabilizing platform that keeps the sensitive axis of the gravimeter aligned with the plumb line. The computational approach usually involves an inertial measurement unit (IMU) that is rigidly attached to the aircraft, which is denoted as a strapdown configuration. Since the IMU contains a triad of gyroscopes and accelerometers, the orientation of the observed specific force can be solved for postmission through the integration of the observed angular rates. This latter approach is commonly denoted as strapdown airborne gravimetry (SAG) and represents the airborne system used in this investigation.

2.1 Filtering and spatial resolution

To subsequently filter the noise in equation (1), we have routinely used a cascaded time-domain implementation of a second-order Butterworth filter at the National Space Institute (DTU Space), part of the Technical University of Denmark (Forsberg et al. 2001). This means that the filter is applied both forwards and backwards in time, resulting in a zero-phase filter with no time lag. Typically, we apply the filter forwards and backwards three times, which we denote as a third stage multipass, second-order Butterworth filter.

The width of the Butterworth filter is defined by a filter time constant (ftc). In order to have a consistent comparison with other filters, the Full-Width-Half-Maximum (FWHM) or Half-Width-Half-Maximum (HWHM) of the curve is often used. However, this can be defined in both temporal and spectral domains. The temporal domain definition is illustrated to the left in Figure 1. In this case, the filter can be applied to a discrete delta function time series (black), resulting in a weight curve with a width that depends on the ftc (red, blue, and yellow). The FWHM or HWHM of the normalized weight curve defines the time-domain resolution of the filter.

In the frequency domain, the transfer function, $H(f)$, can be derived experimentally as follows:

$$|H(f)| = \sqrt{\frac{S_o(f)}{S_i(f)}} = \frac{|\mathcal{F}(y_o)|}{|\mathcal{F}(y_i)|} = \frac{\mathrm{abs}(\,\mathrm{fft}(\mathrm{y_o}))}{\mathrm{abs}(\,\mathrm{fft}(\mathrm{y_i}))}, \tag{2}$$

where y_i denotes the input (delta) function, y_o denotes the filtered output, $S_i(f)$ and $S_o(f)$ denote the power spectral densities thereof, and `fft` denote the fast Fourier transform (the right-most part imitates the numerical implementation). In this case, the half-transmission point, $f_{\frac{1}{2}}$, can be read on the curve as illustrated to the right in Figure 1. The half-transmission point can be converted from the frequency domain to the time domain as follows:

$$\mathrm{FWHM} = 2 \cdot \mathrm{HWHM} = \frac{1}{2f_{\frac{1}{2}}}. \tag{3}$$

In either case, the resolution can be expressed as the FWHM or HWHM, defining the along-track resolution in units of time. The along-track spatial resolution, λ_{FWHM} or λ_{HWHM}, of the resulting gravity estimates is proportional to the along-track velocity of the aircraft, v, as follows:

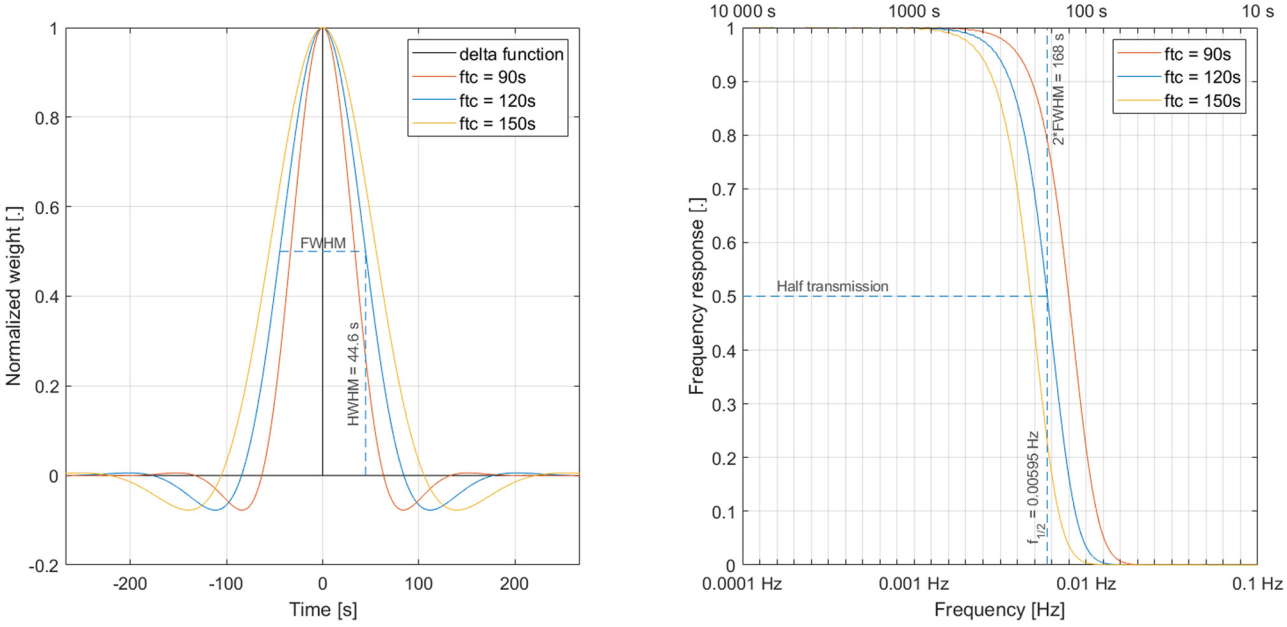

Figure 1: Illustration of third-stage, second-order Butterworth filter with three different time constants of 90, 120, and 150 s applied to a delta function. (Left) Normalized convolution filters. (Right) Transfer functions (more specifically frequency response functions). Note the units of frequency at the bottom and time at the top.

$$\begin{aligned} \lambda_{\mathrm{FWHM}} &= v \cdot \mathrm{FWHM}, \\ \lambda_{\mathrm{HWHM}} &= v \cdot \mathrm{HWHM}. \end{aligned} \tag{4}$$

An example is illustrated in Figure 1. A third-stage, second-order Butterworth filter with a filter time constant of 120 s is applied to a delta function. If the time-domain approach is pursued (left figure), the FWHM temporal resolution is 89 s. At an along-track velocity of 67 m/s, this results in a full-wavelength spatial resolution of 6.0 km and a half-wavelength resolution of 3.0 km. If the spectral-domain approach is pursued (right figure), the half-transmission point is $f_{\frac{1}{2}} = 0.00595$ Hz, leading to an FWHM temporal resolution of 84 s. An along-track velocity of 67 m/s results in a full-wavelength spatial resolution of 5.6 km and a half-wavelength resolution of 2.8 km.

It should be noted that the frequency-domain approach does not generally result in a lower resolution for any filter and time constant. For the remainder of this investigation, the frequency-domain approach is used.

2.2 Processing methodology in strapdown airborne gravimetry

The angular rates and accelerations measured by the IMU will contain systematic errors, such as bias, scale factor, and cross-coupling. For this reason, the IMU observations are usually combined with GNSS observations using a Kalman filter approach. The angular rates are integrated for attitude and the accelerations for velocity and position, whereas independent estimates of position (and possibly velocity) are derived from GNSS observations. These estimates are combined in a statistically optimal fashion within the Kalman filter framework by modelling the temporal evolution of an error covariance matrix representing a set of states chosen for the system. The most fundamental states are attitude, velocity, and position along with gyroscope and accelerometer biases (Jekeli 2001, Titterton and Weston 2004, Groves 2013).

The attitude estimates derived from the Kalman filter framework are then used to form the rotation operator in equation (1). This approach to deriving gravity estimates has been denoted as the direct or cascaded approach (Jekeli and Garcia 1997). However, since the measured IMU accelerations are compensated for gravity before integration, it is possible to add additional states, representing the error on the applied gravity field model, to the Kalman filter state vector. In this way, estimates of the gravity vector can be derived directly from the Kalman filter. This approach is sometimes denoted as the indirect or centralized approach. Both methods have been applied with similar results (Johann et al. 2019).

Using the direct approach, it is straightforward to derive the spatial resolution from the half-transmission point of the applied filter. Using the indirect approach,

the degree of filtering is controlled by modelling the variation in the gravity field as a stochastic process. The derived gravity estimates are a result of stochastic modelling and weighting observations in a way that depends on the physical circumstances. It is, therefore, not straightforward to derive the spatial resolution, which may not even be uniform along the survey.

2.3 Spatial resolution from Kalman filter estimates

The spatial resolution of gravity estimates originating from the indirect approach can be estimated similarly to the method described earlier by applying a delta function and forming the frequency response, $|H(f)|$. One approach for experimentally deriving the transfer function is described further.

Figure 2 shows two profiles of vertical gravity disturbance estimates along an airborne gravity survey. The first profile (blue – not visible below the red curve) represents Kalman filter estimates using IMU and GNSS observations with no modifications. The second profile (red) is derived using the exact same processing but with a delta function of 1 mGal amplitude over a single 300 Hz sampling interval applied to the vertical accelerations (after the accelerations have been rotated into a local-level system). Also shown is the difference between the two profiles having a peak of approximately 4×10^{-5} mGal centred around the delta function.

In order to derive the transfer function as described previously, we need to use the input and output functions from the filter. In this case, a delta function time series of 1 mGal amplitude and 300 Hz sampling interval represents the input function, y_i. The difference between the two gravity profiles in Figure 2 represents the output function, y_o. Using these two time series, it is possible to derive the transfer function using equation (2). The associated convolution filter and transfer function is illustrated in Figure 3. By reading off the half-transmission point, the spatial resolution can be derived from the along-track velocity using equations (3) and (4).

3 Survey and data

The data used in this investigation represent two sources: (1) a gravity database consisting of ground and shipborne gravity observations collected through many years and (2) new airborne gravity observations collected on April 25th 2016 during a test flight of the iNAT-RQH navigation-grade IMU from iMAR navigation.

An overview of the database and flight track is shown in Figure 4. The survey was initiated from Roskilde Airport (RKE) and consisted of a single flight line flown twice. The line was arranged such that the profile

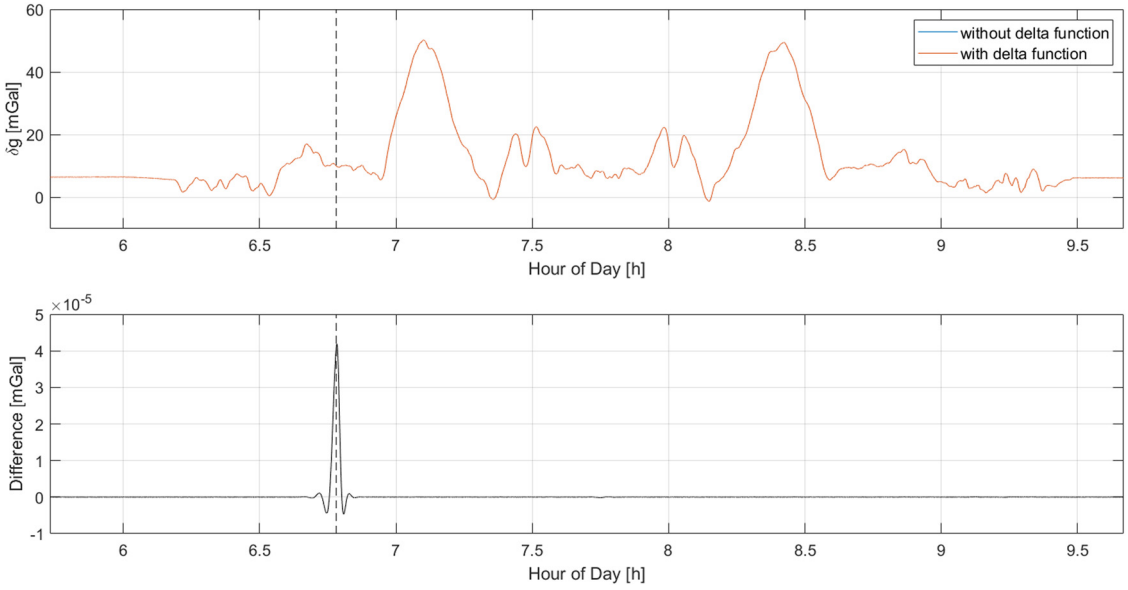

Figure 2: Illustration of vertical gravity estimates with and without applying a delta function of 1 mGal amplitude to the vertical channel of acceleration. The dashed line illustrates where the delta function was applied. (Top) Gravity disturbance estimates with and without applying a delta function (difference not visible – red curve is on top of the blue curve). (Bottom) Difference between the two estimated gravity profiles.

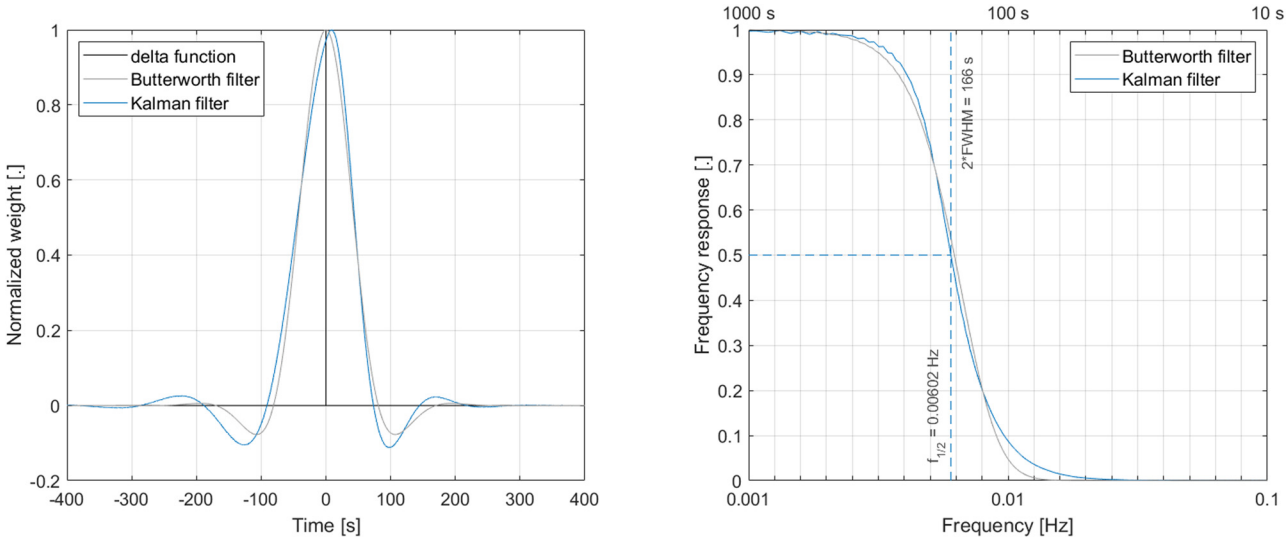

Figure 3: Illustration of the normalized weight function and transfer function derived from the differences shown in Figure 2. Also shown are the curves derived from a third-stage, second-order Butterworth filter with a time constant of 115 s. (Left) Normalized convolution filter. (Right) Transfer function.

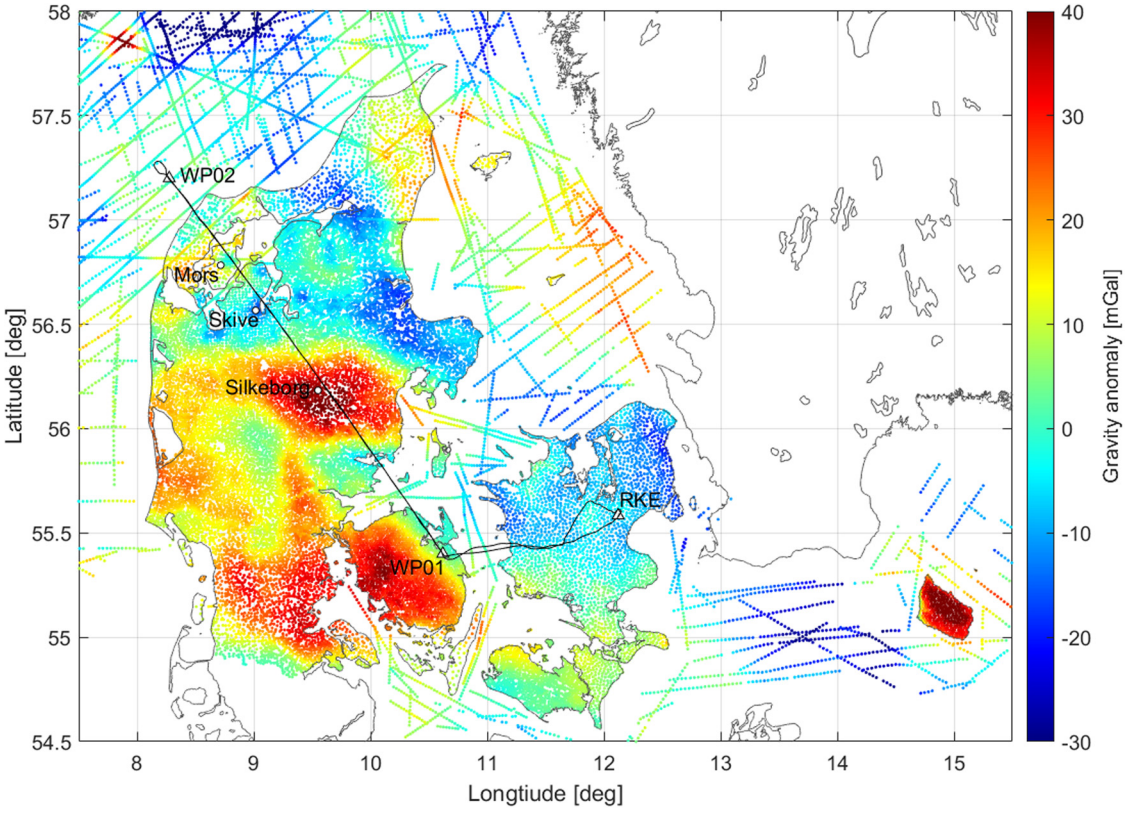

Figure 4: Overview of the survey. The ground track (black) is illustrated along with gravity anomalies measured across the region. Also shown is Roskilde Airport (RKE), the two waypoints defining the flight line and some relevant locations along the line.

crosses over the Silkeborg gravity high and the Danish Salt Dome Province in northwestern Jutland (Madirazza et al. 1990, Ramberg and Lind 1968). The two waypoints are approximately 300 km apart, and the profile was flown at an altitude of around 600 m (2,000 ft.) and a ground speed of 67 m/s (130 kts).

3.1 Upward continuation of ground observations

To compare the database gravity values with airborne estimates, the ground gravity anomalies, Δg, are converted to gravity disturbances, δg, as follows:

$$\delta g = \Delta g + N \cdot 0.3086 \text{ mGal/m}, \quad (5)$$

where N is the geoidal undulation. Using the GRAVSOFT software package, the gravity disturbances are interpolated onto a $0.005^\circ \times 0.01^\circ$ grid using least squares collocation, with the covariance modelled as a second-order Gauss–Markov model having a correlation length of 25 km. Afterwards, the grid is upward continued to an altitude of 600 m using the fast Fourier transform and interpolated onto the flight trajectory (Schwarz et al. 1990). The resulting gravity profile is illustrated together with the airborne estimates in Figure 5.

3.2 Airborne gravity processing

For the airborne survey, the IMU was installed together with a JAVAD DELTA GNSS receiver and some batteries on the back seat of a Cessna 182T Skylane aircraft. A NovAtel ANT-532-C dual frequency GNSS antenna was attached to the rear windscreen of the aircraft using tape and connected to the GNSS receiver.

Using the Hexagon | NovAtel Waypoint software suite, a PPP solution was derived from the GNSS observations together with final satellite ephemeride products made available by the International GNSS Service. A temperature drift correction as described by Becker et al. (2015) was applied to the vertical accelerometer readings of the IMU. The accelerations and angular rates observed by the IMU were then integrated for attitude, velocity, and position and combined with GNSS position estimates using an extended Kalman Filter approach as described in the study of Jensen & Forsberg (2018). An overview of the stochastic models used in the Kalman filter is given in Table 1.

The along-track variation in gravity disturbance was modelled as a third order Gauss–Markov process, and tie values were introduced before and after take-off as measurement updates. The spatial parameters were transformed into the time domain using combined GNSS/IMU along-track velocity estimates. Finally, the navigation estimates were smoothed by combining navigation profiles processed forward and backward in time using an implementation of the Rauch–Tung–Striebel algorithm (Gelb, 2013, Chapter 5). The resulting vertical gravity disturbance estimates are shown in Figure 5.

4 Results

The spatial resolution of the airborne gravity estimates derived using Kalman filtering is estimated using two

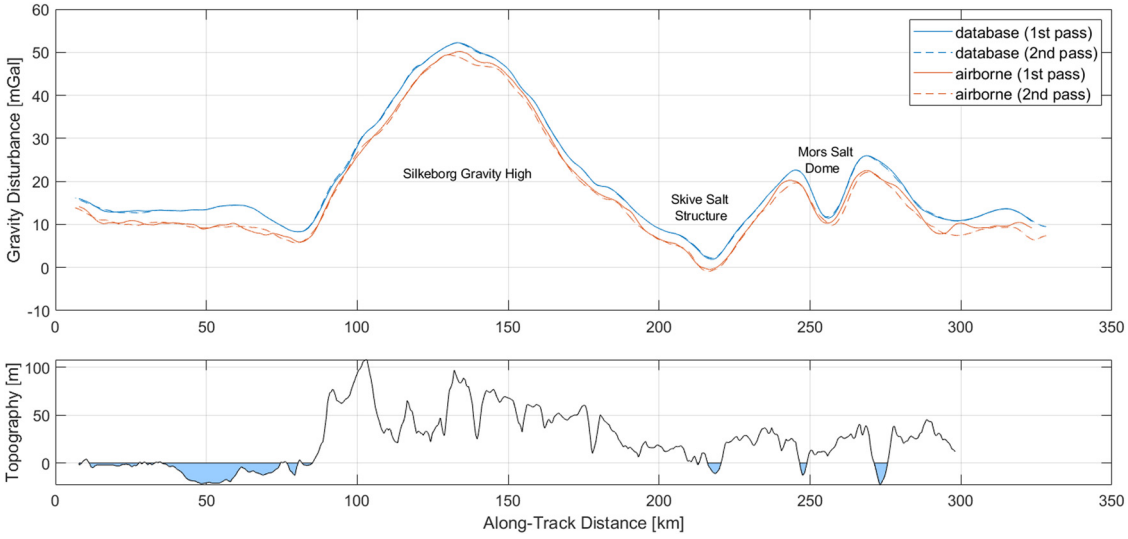

Figure 5: Gravity and topography along the profile. (Top) Gravity disturbance from the first and second flight pass. Blue lines are upward continued ground observations; red lines are airborne gravity estimates; (Bottom) Along-track topography from the 30 arc second Shuttle Radar Topography Mission (SRTM30) data product (Farr and Kobrick 2011).

Table 1: Overview of error states modelled in the extended Kalman filter

Error state	Model	Initial uncertainty	System noise
Attitude	Random walk	[1, 1, 5]°	0.2 arcsec/$\sqrt{s}$
Velocity	Random walk	0.5 m/s	5×10^{-5} m/s/$\sqrt{s}$
Position	None	[1, 1, 5] m	0 m/$\sqrt{s}$
Gyroscope bias	Random constant	0.001°/h	0° /h/$\sqrt{s}$
Accelerometer bias	Random walk	30 mGal	0.01 mGal/$\sqrt{s}$
Gravity disturbance	Third order Gauss–Markov model	0.03 mGal	σ = [11.66, 5.05, 13.62] mGal
			$1/\beta$ = [5790, 9470, 7210] m

methods: (1) The resolution is estimated based on a comparison with the upward continued terrestrial observations; (2) The resolution is estimated using the method proposed earlier by applying a delta function to the observed accelerations and forming the transfer function.

4.1 Comparing airborne and ground observations

The gravity database and airborne gravity estimates represent two independent sources of information that can be compared. By forming the difference between the two profiles, the mean, minimum, maximum, standard deviation (STD), root-mean-square (RMS) and root-mean-square-error (RMSE = RMS/$\sqrt{2}$) measures can be derived from the residuals. These are shown in the first two rows of Table 2.

Comparing airborne gravity estimates from the first and second pass of the profile represents an internal validation of the airborne estimates. This is shown in the third row of Table 2, whereas the fourth row represents statistical variables derived from the difference between upward continued gravity values interpolated to the first and second pass, respectively. In this case, the deviation originates purely from differences in position, since the trajectories differ slightly.

By assuming that the upward continued database profile resembles the actual non-smoothed gravity field at flight altitude, we can use the profile to estimate the spatial resolution of the airborne gravity estimates. If we pretend that the airborne gravity estimates were filtered using a third-stage, second-order Butterworth filter, we can apply this filter with varying filter time constants, in order to find the smoothed profile that best resembles the airborne gravity estimates. Figure 6 illustrates the STD and RMS of the residuals between database and airborne estimates, formed after applying an along-track filter to the upward continued database profile. It is noted that the residuals are formed using only that part of the profile which is on the surveyed line segment.

Comparison of the difference between smoothed database and airborne estimates indicates the best agreement between the two profiles using a filter time constant of 115 s. A third-stage, second-order Butterworth filter with a 115 s filter time constant has a half-transmission point at 0.00621 Hz, which can be converted to a full-wavelength resolution of 5.39 km at an along-track velocity of 67 m/s using equation (4).

4.2 Estimating the spatial resolution of gravity estimates

A delta function of 1 mGal amplitude at 300 Hz sampling rate was added to the vertical accelerations during the processing of airborne data. By comparing the resulting gravity estimates with the unperturbed estimates, the

Table 2: Statistical variables derived from differences between gravity profiles (profile 1 minus profile 2)

Profile 1	Profile 2	Mean	Min	Max	STD	RMS	RMSE	
First pass database	First pass airborne	2.5	0.6	5.5	0.9	2.7	1.9	mGal
Second pass database	Second pass airborne	3.0	0.9	5.0	0.7	3.0	2.2	mGal
First pass airborne	Second pass airborne	0.4	−1.2	2.8	0.7	0.8	0.6	mGal
First pass database	Second pass database	0.0	−0.6	0.6	0.2	0.2	0.1	mGal

RMS refers to the root-mean-square and RMSE = RMS/$\sqrt{2}$ to the root-mean-square-error. There are two data sources and the line profile was flown twice, resulting in four possible combinations.

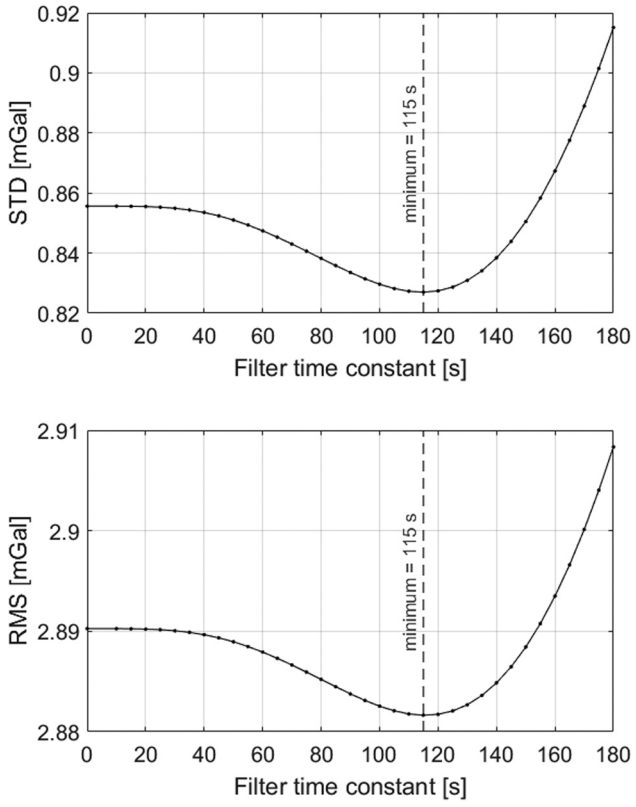

Figure 6: STD and RMS of the difference between database and airborne gravity estimates after applying a third-stage, second-order Butterworth filter of varying filter time constant to the upward continued database profile. The residuals are formed only for that part of the profile which is on the surveyed line segment.

spatial resolution was derived according to the method described in Section 2.3. This procedure was repeated 57 times at approximately 120 s intervals, adding only a single delta function at each processing iteration. The derived spatial resolution along the two passes of the line is shown in Figure 7. The mean value of 5.54 km has an STD of 0.14 km.

5 Discussion

From the results presented in the previous section, it is evident that the method proposed in this investigation yields results consistent with the database comparison, namely a full-wavelength spatial resolution of approximately 5.5 km.

Inspecting Figure 7 there is also evidence that the spatial resolution is not constant throughout the profile. This is consistent with expectations as argued previously. The average spatial resolution for the first pass of the profile is 5.49 km, whereas the average for the second pass is 5.59 km, indicating that spatial resolution is dependent on physical circumstances such as weather conditions, flight dynamics and GNSS observability.

Comparing database and airborne estimates in Table 2, the mean value indicates an offset between the two datasets. Since the IMU was not strictly fixated on the aircraft during this test flight, this bias could easily originate from a physical movement of the sensor. When interpreting the results, we should also keep in mind that long-wavelength errors mainly arise from the long-term instability of the accelerometers.

Comparing the two datasets in terms of STD, which takes into account a mean difference, the second pass yields results superior to the first pass. This could be due to a difference in filtering since the second pass seems to be subject to more severe filtering, which could result in better accuracy (at the cost of spatial resolution).

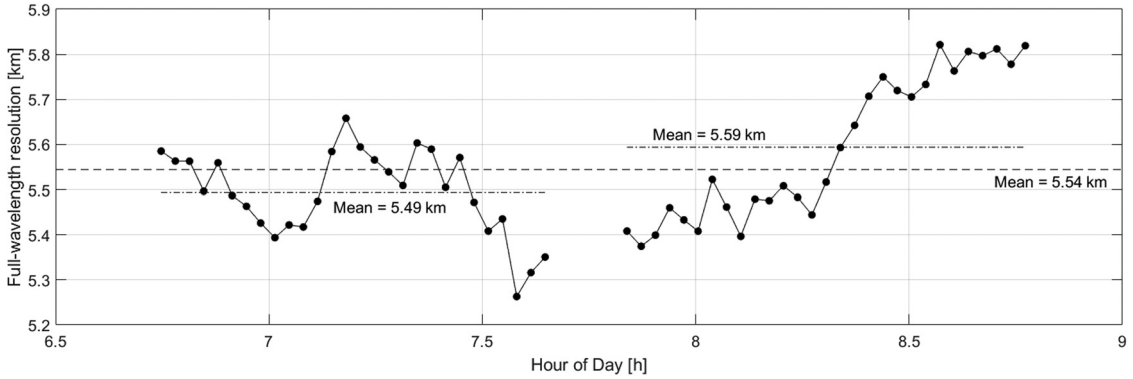

Figure 7: Derived spatial resolution along the two line profiles. Also shown is the mean value of 5.54 km for both passes and mean values of 5.49 and 5.59 km for the first and second pass, respectively.

In terms of the internal validation by comparing airborne estimates from the first and second flight passes, a mean difference of 0.4 mGal is observed. This is consistent with the 0.5 mGal difference when comparing the first and second passes with the database and represents some long-term errors in the gravity estimates, possibly originating from uncompensated drift of the accelerometers.

The estimated accuracy derived by internal validation is 0.6 mGal in terms of the RMSE measure and 0.7 mGal in terms of the STD. When compared with the database, the values are 1.9–2.2 and 0.7–0.9 mGal, respectively. Based on the comparison of database values between the two passes, around 0.1–0.2 mGal originate from the difference in flight trajectory, i.e. comparing gravity estimates at two different locations.

6 Conclusion

This investigation presented a method for deriving spatial resolution of airborne gravity estimates by applying a delta function to the observed accelerations and evaluating the resulting transfer function. The method yields a full-wavelength spatial resolution of approximately 5.5 km at an accuracy of 0.6 mGal, consistent with a comparison with terrestrial observations (ignoring the offset between the datasets).

Acknowledgement: The flight test was organized by Prof. Rene Forsberg from the National Space Institute DTU Space. Arne V. Olsen from Westergard Geo Solutions participated in the flight test. Funding for the survey and study was provided by DTU Space and the Danish Agency for Data Supply and Infrastructure.

Conflict of interest: The author states no conflict of interest.

References

Becker, D., J. E. Nielsem, D. Ayres-Sampaio, R. Forsberg, M. Becker, and L. Bastos. 2015. Drift reduction in strapdown airborne gravimetry using a simple thermal correction. *Journal of Geodesy* 89, 1133–1144, doi: https://doi.org/10.1007/s00190-015-0839-8.

Brozena, J. M. 1992. The Greenland aerogeophysics project: Airborne gravity, topographic and magnetic mapping of an entire continent. In: *From Mars to Greenland: Charting Gravity With Space and Airborne Instruments. International Association of Geodesy Symposia*, edited by Colombo, O. L., vol. 110, New York, NY: Springer, doi: https://doi.org/10.1007/978-1-4613-9255-2_19.

Bruton, A. 1997. Reduction of GPS receiver noise using adaptive filters. In: *Proceedings of the 10th International Technical Meeting of the Satellite Division of The Institute of Navigation*, Kansas City, MO, September 1997, pp. 645–663.

Childers, V. A., R. E. Bell, and J. M. Brozena. 1999. Airborne gravimetry: An investigation of filtering. *Geophysics* 64, 61–69, doi: https://doi.org/10.1190/1.1444530.

Farr, T. G. and M. Kobrick. 2011. Shuttle radar topography mission produces a wealth of data, *Eos Transactions, American Geophysical Union* 81(48), 583–585, doi: https://doi.org/10.1029/EO081i048p00583.

Fauzi Nordin, A., H. Jamil, M. Noor Isa, A. Mohamed, S. Hj. Tahir, B. Musta, R. Forsberg, A. V. Olesen, J. E. Nielsen, A. Majid A. Kadir, A. Fahmi Abd Majid, K. Talib, and S. Aman Sulaiman. 2016. Geological mapping of Sabah, Malaysia, using airborne gravity survey. *Borneo Science* 37(2), 14–27.

Forsberg, R., A. V. Olesen, L. Bastos, A. Gidskehaug, U. Meyer, and L. Timmen. 2000. Airborne geoid determination. *Earth, Planets and Space* 52, 863–866, doi: https://doi.org/10.1186/BF03352296.

Forsberg, R., A. V. Olesen, and K. Keller. 2001. Airborne gravity survey of the North Greenland continental shelf. In: *Gravity, Geoid and Geodynamics 2000. International Association of Geodesy Symposia*, edited by Sideris, M. G., vol. 123, Springer, Berlin, Heidelberg, doi: https://doi.org/10.1007/978-3-662-04827-6_39.

Forsberg, R., A. V. Olesen, K. Keller, M. Moooooller, A. Gidskehaug, and D. Solheim. 2001. Airborne gravity and geoid surveys in the Arctic and Baltic seas. In: *Proceedings of International Symposium on Kinematic Systems in Geodesy, Geomatics and Navigation* (*KIS-2001*), p. 586–593. Banff.

Forsberg R., A. V. Olesen, E. Nielsen, and I. Einarsson. 2015. Airborne gravimetry for geoid and GOCE. In: *IGFS 2014. International Association of Geodesy Symposia*, edited by Jin S., and R. Barzaghi, vol. 144, Springer, Cham, doi: https://doi.org/10.1007/1345_2015_47.

Gelb, A. 2013. *Applied optimal estimation*, The M.I.T Press, Cambridge, MA, USA and London, England, ISBN 0-262-20027-9.

Groves, P. D. 2013. *Principles of GNSS, inertial, and multisensor integrated navigation systems*, 2nd Edition, Artech House, ISBN 978-1608070053.

Gumert W., V. Graterol, G. Washcalus, and J. Kratochwill. 1991. Airborne gravity surveying an effective exploration tool. In: *Kinematic Systems in Geodesy, Surveying, and Remote Sensing. International Associated of Geodesy Symposia*, edited by Schwarz, K. P., and G. Lachapelle, vol. 107, New York, NY: Springer, doi: https://doi.org/10.1007/978-1-4612-3102-8_49.

Hammada, Y. 1996. *A Comparison of Filtering Techniques for Airborne Gravimetry*, M.Sc. Thesis, Department of Geomatics Engineering, The University of Calgary, UCGE Report No. 20089, doi: http://dx.doi.org/10.11575/PRISM/22591.

Huang J., S. A. Holmes, D. Zhong, M. Véronneau, Y. Wang, J. W. Crowley, X. Li, and R. Forsberg. 2017. Analysis of the GRAV-D airborne gravity data for geoid modelling. In: *International Symposium on Gravity, Geoid and Height Systems 2016.*

International Association of Geodesy Symposia, edited by Vergos G., R. Pail, R. Barzaghi, 148, Springer, Cham, doi: https://doi.org/10.1007/1345_2017_23.

Hwang, C., Y. S. Hsiao, H. C. Shih, M. Yang, K. H. Chen, R. Forsberg, and A. V. Olesen. 2007. Geodetic and geophysical results from a Taiwan airborne gravity survey: Data reduction and accuracy assessment. *Journal of Geophysical Research* 112, B04407, doi: https://doi.org/10.1029/2005JB004220.

Jekeli, C. and R. Garcia. 1997. GPS phase accelerations for moving-base vector gravimetry. *Journal of Geodesy* 71, 630–639, doi: https://doi.org/https://doi.org/10.1007/s001900050130.

Jekeli, C. 2001. *Inertial navigation systems with geodetic applications*, Walter de Gruyter, Berlin, New York, ISBN 3-11-015903-1.

Jensen, T. E. and R. Forsberg. 2018. Helicopter test of a strapdown airborne gravimetry system. *Sensors* 18(9), 3121, doi: https://doi.org/10.3390/s18093121.

Johann, F., D. Becker, M. Becker, R. Forsberg, and M. Kadir. 2019. The direct method in strapdown airborne gravimetry – a review. *Zeitschrift für Geodäsie, Geoinformation und Land management*, 5/2019, doi: https://doi.org/https://doi.org/10.12902/zfv-0263-2019.

Kern, M., Schwarz, K. P., and Sneeuw, N. 2003. A study on the combination of satellite, airborne, and terrestrial gravity data. *Journal of Geodesy* 77, 217–225, doi: https://doi.org/10.1007/s00190-003-0313-x.

Lu, B., F. Barthelmes, M. Li, C. Förste, E. S. Ince, S. Petrovic, F. Fletchner, J. Schwabe, Z. Luo, B. Zhong, and K. He. 2019, Shipborne gravimetry in the Baltic Sea: data processing strategies, crucial findings and preliminary geoid determination tests. *Journal of Geodesy* 93, 1059–1071, doi: https://doi.org/10.1007/s00190-018-01225-7.

Madirazza, I., B. H. Jacobsen, and N. Abrahamsen. 1990. Late Triassic tectonic evolution in northwest Jutland. *Bulletin of the Geological Society of Denmark* 38, 77–84.

Muis, S., M. Verlaan, R. J. Nicholls, S. Brown, J. Hinkel, D. Lincke, A. T. Vafeidis, P. Scussolini, H. C. Winsemius, and P. J. Ward. 2017. A comparison of two global datasets of extreme sea levels and resulting flood exposure. *Earth's Future* 5, 379–392, doi: https://doi.org/10.1002/2016EF000430.

National Research Council of the National Academies. 2009. *Mapping the Zone: Improving Flood Map Accuracy*, The National Academies Press, 500 Fifth Street, N.W. Washington, DC, USA, ISBN 0-309-13058-1.

Novák, P., M. Kern, K. P. Schwarz, M. G. Sideris, B. Heck, S. Ferguson, Y. Hammada, and M. Wei. 2003. On geoid determination from airborne gravity. *Journal of Geodesy* 76, 510–522, 510–522, doi: https://doi.org/10.1007/s00190-002-0284-3.

Ramberg, I. and G. Lind. 1968. Gravity measurements on the Paarup salt dome. *Bulletin of the Geological Society of Denmark* 18, 221–240.

Scheinert, M., F. Ferraccioli, J. Schwabe, R. Bell, M. Studinger, D. Damaske, W. Jokat, N. Aleshkova, T. Jordan, G. Leitchenkov, D. D. Blankenship, T. M. Damiani, D. Young, J. R. Cochran, and T. D. Richter. 2016. New Antarctic gravity anomaly grid for enhanced geodetic and geophysical studies in Antarctica. *Geophysical Research Letters* 43, 600–610, doi: https://doi.org/10.1002/2015GL067439.

Schwarz, K. P. and Z. Li. 1997. An introduction to airborne gravimetry and its boundary value problems. In: *Geodetic Boundary Value Problems in View of the One Centimeter Geoid. Lecture Notes in Earth Sciences*, edited by Sansó, F., R. Rummel , 65, Springer, Berlin, Heidelberg, doi: https://doi.org/10.1007/BFb0011709.

Schwarz, K. P., M. G. Sideris, and R. Forsberg. 1990. The use of FFT techniques in physical geodesy. *Geophysical Journal International* 100(3), 485–514, doi: https://doi.org/10.1111/j.1365-246X.1990.tb00701.x.

Sproule D. M., A. H. W. Kearsley, and M. B. Higgins. 2001. Impact of BRAGS'99 airborne gravimetric data on geoid computations in Australia, and possibilities for utilisation of bathymetric information. In: *Gravity, Geoid and Geodynamics 2000. International Association of Geodesy Symposia*, edited by Sideris M. G., vol. 123, Springer, Berlin, Heidelberg, doi: https://doi.org/10.1007/978-3-662-04827-6_38.

Stepanov, O. A., D. A. Koshaev, and A. V. Motorin. 2015. Identification of gravity anomaly model parameters in airborne gravimetry problems using nonlinear filtering methods. *Gyroscopy and Navigation*, 6, 318–23, doi: https://doi.org/10.1134/S2075108715040136.

Titterton, D. H. and J. L. Weston. 2004. *Strapdown Inertial Navigation Technology*, 2nd Edition. Institution of Electrical Engineers, ISBN 0-86341-358-7.

Vaníček, P. and R. Kingdon. 2015. *Gravimetry*. Reference Module in Earth Systems and Environmental Sciences, Elsevier, doi: https://doi.org/10.1016/B978-0-12-409548-9.09145-4.

Zhou, W. and T. J. Cai. 2013. Study on filtering methods of airborne gravity. *Applied Mechanics and Materials* 333–335, 516–521, doi: https://doi.org/10.4028/www.scientific.net/amm.333-335.516.